Electrowetting Control of Cassie-to-Wenzel Transitions in Superhydrophobic Carbon Nanotube-Based Nanocomposites

Zhaojun Han,[†,‡] Bengkang Tay,[†] Cherming Tan,[†] Maziar Shakerzadeh,[†] and Kostya (Ken) Ostrikov[‡,§,*]

[†]School of Electrical and Electronic Engineering, Nanyang Technological University, 639798 Singapore, [‡]CSIRO Materials Science and Engineering, P.O. Box 218, Lindfield, New South Wales 2070, Australia, and [§]School of Physics, The University of Sydney, Sydney NSW 2006, Australia

ABSTRACT The possibility of effective control of the wetting properties of a nanostructured surface consisting of arrays of amorphous carbon nanoparticles capped on carbon nanotubes using the electrowetting technique is demonstrated. By analyzing the electrowetting curves with an equivalent circuit model of the solid/liquid interface, the long-standing problem of control and monitoring of the transition between the "slippy" Cassie state and the "sticky" Wenzel states is resolved. The unique structural properties of the custom-designed nanocomposites with precisely tailored surface energy without using any commonly utilized low-surface-energy (*e.g.*, polymer) conformal coatings enable easy identification of the occurrence of such transition from the optical contrast on the nanostructured surfaces. This approach to precise control of the wetting mode transitions is generic and has an outstanding potential to enable the stable superhydrophobic capability of nanostructured surfaces for numerous applications, such as low-friction microfluidics and self-cleaning.

KEYWORDS: carbon nanotube · nanocomposites · superhydrophobic · Cassie-to-Wenzel transition · electrowetting

Solid surfaces with controllable wettability are promising for applications such as microfluidics, oil degreasing, painting, molecular filtration, cell adhesion, and drug delivery.[1−4] In contrast to smooth surfaces which often have a maximum contact angle not exceeding 120° and thus a narrow range for the dynamic control of surface wettability, nanostructured surfaces have recently drawn considerable interest because of their capability to achieve more effective and flexible control properties ranging from superhydrophobicity (contact angle >150°) to superhydrophilicity (contact angle <20°).[5−7] Superhydrophobic nanostructured surfaces exist naturally (*e.g.*, lotus leaf) and can also be designed through precise tailoring of the surface roughness/texture at the nanoscales.[7−9]

The Wenzel and Cassie mechanisms are commonly invoked to explain the observed superhydrophobic properties of the surfaces.[10,11] The Wenzel mechanism plays a role when the surface is gently roughened and the relatively large surface areas lead to significant water-repellent responses. In this case, the contact angle is enhanced by $\cos\theta = r\cos\theta_0$ (θ is the measured contact angle, θ_0 is the angle on a smooth surface, and r is the nondimensional surface roughness).[10] The Cassie mechanism, in turn, is applicable to the cases when the surface has a relatively high roughness. It was suggested that in this case air bubbles can be trapped below the droplet, resulting in larger contact angles given by $\cos\theta = \phi_S(1 + \cos\theta_0) - 1$, where ϕ_S is the fraction of solid in contact with the liquid.[11] Figure 1a shows the plots of both the Cassie (blue line) and the Wenzel (red line) wetting curves along with the changes in hydrophobicity of smooth surfaces.

In many cases, however, liquid droplets residing on nanostructured surfaces are in a metastable Cassie state. When the surfaces are slightly hydrophobic (θ_0 just above 90°), θ_0 is less than the critical value θ_C, which is defined by the intersection between the Cassie and the Wenzel lines (Figure 1a). Under these conditions, the Cassie state is metastable (dotted line) and the Wenzel state is the minimum energy state (Figure 1a). A transition for the droplet from the metastable Cassie state to the stable Wenzel state is possible if external stimuli such as temperature, compression, vibration, impact, and electrostatic interactions are provided to overcome the associated energy barrier.[12−16] It is known that although both Cassie and Wenzel states can enable surface hydrophobicity, their dynamic wetting behaviors are very different. The contact angle hysteresis (the difference between the advancing and the receding

a

b
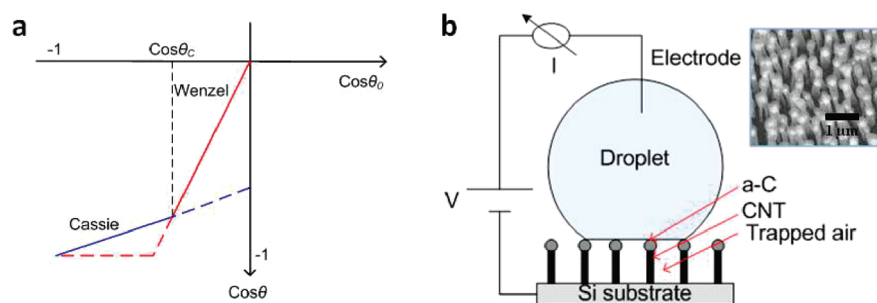
Figure 1. (a) The plots of the Cassie and the Wenzel angles as a function of the contact angle on smooth surfaces. Liquid droplets residing on the solid surface are in the metastable Cassie state if surface hydrophobicity has a contact angle less than the critical angle θ_C, which is the intersection between the Cassie and the Wenzel angles. (b) The schematic diagram for electrowetting setup. The droplet is in contact with the *a*-C nanoparticles and air is trapped between neighboring CNTs in the Cassie state. The inset shows the microstructure of *a*-C/CNT nanocomposites.

angles) is usually low for liquid droplets in the Cassie state but can be over 100° for the Wenzel state.[12] The droplets can therefore move freely in the Cassie state (*i.e.*, "slippy" state) but usually remain "pinned" in the Wenzel state (*i.e.*, "sticky" state). In addition, the contact area between the liquid and the solid surface is also increased along with the transition, which possibly affects the interfacial adhesion behaviors. Therefore, a simple technique that can characterize the Cassie-to-Wenzel transition on nanostructured surfaces is highly desirable to avoid the unwanted sticking transition in water-repellent applications such as low-friction microchannels, self-cleaning, antifouling, *etc*.

To solve this problem, we have custom-designed and synthesized superhydrophobic carbon nanotube (CNT)-based nanocomposites and employed the electrowetting technique to control the surface wettability. The microstructure of the nanocomposites shows arrays of spherical amorphous carbon (*a*-C) nanoparticles (~100 nm thick) capped on CNTs, *i.e.*, forming *a*-C/CNT nanocomposites (Supporting Information S1 and S2).[17] The diameter of CNTs ranges from 50–200 nm and the diameter of the *a*-C caps is slightly larger than that of CNTs, giving an "overhang" structure. The height of *a*-C/CNT is about 1–2 μm and the average intertube distance is about 300 nm. These nanocomposites were prepared using the plasma/ion-aided deterministic nanofabrication and were not deliberately conformally coated with fluoropolymers (or any other low-surface-energy coatings), which is commonly used to enhance hydrophobicity.[18] The mechanism of electrowetting is that when a potential is applied between the liquid and the solid, the charges and dipoles redistribute to reduce the interfacial energy, leading to an increase in surface wettability.[19] Electrowetting has been successfully applied to control surface wettability as well as to manipulate tiny amount of liquids on surfaces, without changing surface composition and structure. In this way, liquids with high surface tension (*e.g.*, mercury) can be filled into nanoscale channels and nonwetting polymers can be infiltrated into the CNT forest.[20,21] As

compared to other techniques, electrowetting is advantageous in controlling surface wettability due to its simplicity, efficiency, and fast response.

RESULTS AND DISCUSSION

To demonstrate the superhydrophobicity of the custom-made *a*-C/CNT nanocomposites, a deionized (DI) water droplet (10 μL) was dispensed on the surface and a contact angle of approximately 160° was achieved, as measured by the static sessile drop method. This droplet could easily roll off from the surface with a slight tilting angle (<5°), indicating that it was in the Cassie state where air bubbles were trapped in the gaps between neighboring CNTs (Supporting Information S3). The Cassie state is supported due to the "overhang" structure of *a*-C/CNTs, although *a*-C nanoparticles on the top surface have a moderate hydrophobicity (the contact angle does not exceed 90°).[22] It was shown that in this structure, because the liquid–air interface between the neighboring nanotubes would have to deform considerably to exceed a large advancing contact angle, droplets could hardly penetrate into the internanotube gaps unless a high pressure (~10⁴ Pa) was applied (Supporting Information S3).[22] In contrast, for uncapped CNT forests without the "overhang" structure, nearly complete wetting can be observed as water effectively seeps into the gaps (Supporting Information S4).[23]

The electrowetting setup is schematically shown in Figure 1b. When a DI water droplet is dispensed on the surface, an electric field is applied to the droplet by inserting a Ti/Ni electrode wire and to the supporting substrate (n-type Si, resistivity 0.01–0.03 Ω·cm) of the *a*-C/CNT nanocomposites, respectively. The thin *a*-C layer in the nanocomposites serves as a dielectric layer to block the current flow, whereas the underlying CNTs remain conducting, which is a typical structure for electrowetting-sensitive devices. Previous work has shown that the positive potential applied to the CNTs and the negative potential applied to the droplet caused strong electrochemical oxidation of the CNTs and, eventually, an abrupt switching from the nonwetting to the wetting state.[24] To avoid this, we have applied a negative potential to the substrate and a positive potential to the droplet. Indeed, no abrupt change in wetting states was observed throughout the experiments.

Figure 2a shows typical contact angle images for droplets measured at different applied potentials. The contact angles were found to reduce at voltages as low as 9 V. As the applied potential increased, the angles decreased further in a nonreversible fashion and the drop-
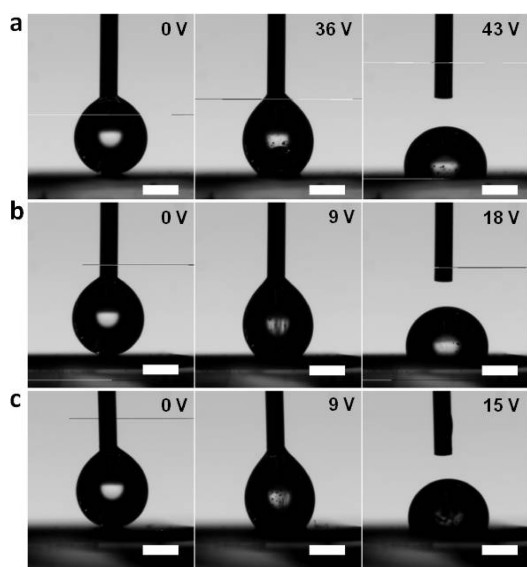
Figure 2. The electrowetting images for different liquids at different potential: (a) DI water, (b) 0.05 M NaCl, and (c) 0.1 M NaCl. The scale bar is 1 mm for all images.

lets tended to detach from the top electrode (a distance of 2 mm to the solid surface). Both the effects of the gravity force and the hydrostatic pressure exerted by the droplet on the substrate ($\sim 10^2$ Pa) are weak in the current case, therefore not affecting the electrowetting effect.[12] At a voltage of 43 V, the droplet was fully detached and a stable angle of 104° with an interfacial area of approximately 2 mm in diameter between the droplet and the surface was observed (Figure 2a). These observations are substantially different from electrowetting on smooth surfaces where a rapid contact angle saturation was reported.[19] In this series of experiments, no contact angle saturation has been observed in the whole range of the applied potentials. The hydrophilic or even superhydrophilic regime can be achieved by reducing the distance between the electrode and the solid surface and increasing the applied voltage. These results are also quite different from electrowetting on densely packed CNT forests, where an abrupt transition from the superhydrophobicity to the complete wetting occurred when the applied potential was higher than a threshold value.[24−26]

An electrolyte of 0.05 M NaCl solution was then used to replace the DI water to simulate the biological saline solutions in contact with the nanostructured surfaces. The same electrowetting process was applied. In this case, the angles reduced much faster than in the DI water case, as shown in Figure 2b. In fact, the angles started to decrease at a very low surface potential and the droplet detached from the electrode at potentials as low as 18 V. Further increasing the concentration of the electrolyte to 0.1 M NaCl only changed the angles slightly, as shown in Figure 2c.

The above observations have been examined using the Lippmann equation for electrowetting with an equivalent circuit model of the liquid/solid interface. It

is known that the contact angles depend on the applied potential according to the Lippmann equation[19,21]

$$\cos \theta_V = \cos \theta_0 + \frac{C}{2\gamma_L} V_A^2$$

where θ_V and θ_0 are the angles with and without the applied potential V_A, C is the capacitance at the interface, and γ_L is the surface energy of the liquid droplet. In the present case, using the Randle-type equivalent circuit model of the liquid/solid interface, the interfacial capacitance C at the equilibrium state consists of the three parts, namely, C_{EDL}, $C_{a\text{-}C}$, and C_{air}, which are the capacitances of the electric double layer (EDL), the a-C nanoparticles, and the trapped air, respectively (Figure 3b). The capacitances of $C_{a\text{-}C}$ and C_{air} can be determined from the geometry of the nanostructured surface and are independent of the droplet (note that because the trapped air occupies a large portion of interfacial area, it can contribute significantly to the interfacial capacitance and hence the electrowetting behaviors (see also ref 27)). On the other hand, C_{EDL}, which is dependent on the thin electric sheath in the vicinity of the solid surface, can be strongly affected by both the ionic concentration of the droplet and the applied potential.[28]

The plots of $\cos \theta_V$ as a function of V_A^2 for all liquids used in the experiments are shown in Figure 3a. For DI water, two different regimes have been identified; these regimes are separated by the potential $V_A = 36$ V. In the first regime where the potential increased from 0 to 36 V, the contact angles decreased slowly from 160° to 142°. In the second regime, however, the angles decreased much faster and the droplet fully detached from the electrode with a final angle of 104° at 43 V. This indicates that the droplet in the first regime was in the Cassie state, as justified by the high contact angles and the low contact angle hysteresis. The small
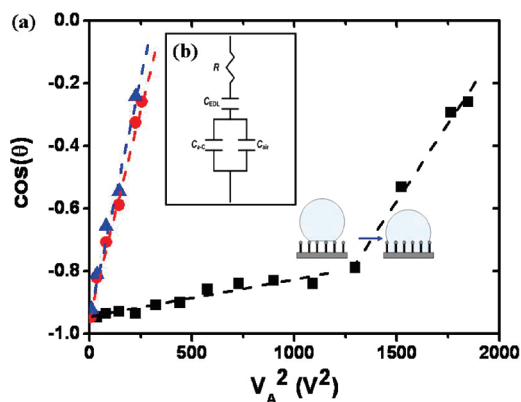
Figure 3. (a) The plots of $\cos \theta_V$ as a function of the squared applied potential V_A^2 for DI water (■), 0.05 M NaCl (●), and 0.1 M NaCl (▲). Dashed lines are linear fits for the corresponding measurements. The Cassie-to-Wenzel transition occurred at the threshold value $\theta_V \approx 142°$. (b) The Randle-type equivalent circuit model of the liquid/solid interface. C_{EDL}, $C_{a\text{-}C}$, and C_{air} are the interfacial capacitance for the electric double layer, the a-C nanoparticles and the trapped air, respectively.
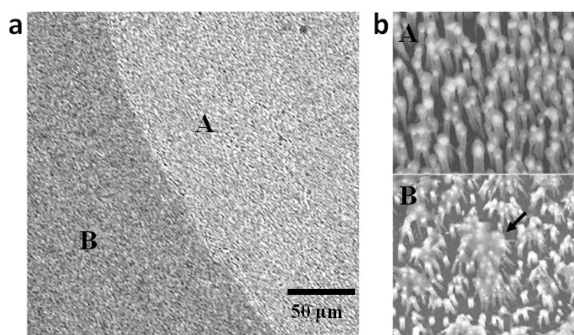
Figure 4. (a) The optical graph at the boundary of an evaporated electrolyte droplet. Region A is light gray color denoting the electrowetted region and region B is dark gray color denoting the unwetted region. (b) The scanning electron micrographs for regions A and B. Arrow in B points to NaCl nanocrystals condensed on top of the *a*-C/CNT bundles.

interfacial capacitance between the liquid and the solid surface in this state led to a relatively weak electrowetting effect and hence slow changes in contact angles, consistent with the observations. On the other hand, when the contact angle was reduced to a threshold value ($\theta_V \approx 142°$) at the elevated potential, strong electrocapillary forces pushed the droplet to penetrate into the gaps between neighboring CNTs and propagate further down the CNTs.[21,22] A transition from the superhydrophobic Cassie to the superhydrophobic Wenzel state was therefore induced. The threshold angle here agreed well with Lafuma *et al.* who used a superhydrophobic surface with similar nanostructures.[12] In the Wenzel state, the interfacial capacitance could be of an order of magnitude higher after the transition because water was in contact with the CNTs. A much faster reduction in angles was the case for the large applied potentials, consistent with the observations in the second regime. Nonetheless, as compared to the densely packed CNT forests with a high aspect ratio, the electrowetting effect in the present case is fairly weak due to a relatively small interfacial area between the liquid and the solid surface.[24] This weak electrowetting effect is preferred in certain circumstances because it offers a more flexible control of surface wettability.

The interfacial capacitance could be large for electrolytes at the initial stage due to their large C_{EDL}. Zhu *et al.* measured the capacitance of aligned CNT arrays in contact with the DI water to be 0.017 μF/cm^2, whereas the capacitance of CNT arrays wetted with a 0.03 M NaCl solution was approximately 0.311 μF/cm^2.[21] As shown in Figure 3a, very strong electrowetting effects were observed for 0.05 M NaCl and the Cassie-to-Wenzel transition occurred at a low applied potential ($\theta_V \approx 143°$ at $V_A = 3$ V). A linear fit can therefore be applied to the experimental data in the whole range of the applied potential. A further increase in the concentration of the electrolyte only led to a slight increase in C_{EDL}, therefore weakly affecting the electrowetting effects.

Visualization of the Cassie-to-Wenzel transition is a very delicate process. Indeed, Krupenkin and co-workers employed a UV polymerizable liquid to confirm the Cassie-to-Wenzel transition in the electrowetting processes.[16,22] Under UV irradiation, the liquid became solidified so that the penetration of liquids into the surface can be visualized microscopically. However, this technique is quite tedious and time-consuming.

Here we used another simple visual indication of this wetting mode transition. An unique structural property of CNT forests is that CNTs collapse into bundles upon the evaporation of penetrated water due to capillary forces.[23] Since this effect was also observed for the *a*-C/CNT nanocomposites, it provided an additional reliable justification for the Cassie-to-Wenzel transition. In this case, it is possible to visually distinguish the two different states. We first observed different evaporation modes of droplets with and without electrowetting (Supporting Information S5). For freely dispensed droplets, the evaporation followed the constant-contact-angle mode when the volume was reduced, a phenomenon associated with the Cassie state. However, after electrowetting, the droplets followed the constant-contact-area mode when evaporated, clearly indicating the occurrence of the Wenzel state.[29]

In addition, we compared the optical images taken at the boundary of the evaporated droplet after electrowetting. As shown in Figure 4a, apparently there is an optical contrast between the electrowetted area (light gray color; region **A**) and the unwetted *a*-C/CNT nanocomposites (dark gray color; region **B**). The microstructures in the two regions were also investigated microscopically using scanning electron microscopy (Figure 4b). The vertically aligned *a*-C/CNT nanostructures remained intact in the unwetted area but collapsed into bundles in the electrowetted area. For droplets of NaCl solutions, one can also observe condensed NaCl nanocrystals on top of *a*-C/CNT bundles after the evaporation (pointed by an arrow in Figure 4b). This is in a good agreement with the results that NaCl can be removed from aqueous solutions through electrosorption.[30] In contrast, droplet evaporated from the surface without electrowetting did not reveal any optical contrast.

CONCLUSIONS

In this work we have investigated the electrowetting control of and visualized the Cassie-to-Wenzel transition on the surface of the custom-designed superhydrophobic *a*-C/CNT nanocomposites. By applying a potential between the water droplet and the solid surface, the contact angles reduced from the angles attributed to the superhydrophobic Cassie state owing to the lowered interfacial energy. When the angles approached the threshold value ($\sim$142°), a transition from the "slippy" Cassie to the "sticky" Wenzel state oc-

curred. Subsequently, the larger capacitance in the Wenzel state resulted in a much faster response of the contact angles to the applied potential. An equivalent circuit model that takes account of both the surface microstructure and the electric double layer has also been used to determine the interfacial capacitance for electrowetting with electrolyte. This model further suggests that if the density of CNTs is changed through, for example, lithographic patterning, the interfacial capacitance will be changed and hence the electrowetting behaviors. In addition, the Cassie-to-Wenzel transition was confirmed and monitored by analyzing the optical contrast on the surface after the droplets were evaporated. Our approach demonstrated the electrowetting as a simple, yet effective technique to control surface wettability of superhydrophobic nanostructured surfaces. We believe that the approach used here is viable not only to study the Cassie-to-Wenzel transition but also to enable the stable superhydrophobic capability of nanostructured surfaces for numerous applications, such as low-friction microfluidics and self-cleaning.

EXPERIMENTAL METHODS

Carbon nanotube (CNT) forests were first synthesized by plasma-enhanced chemical vapor deposition (PECVD), a reliable and reproducible process for the controlled growth of many one-dimensional nanostructures such as nanowires and nanotubes.[18,23,31−35] Briefly, a thin catalyst layer (10 nm Ni) was first deposited on a Si wafer (n-type, resistivity $0.01-0.03\ \Omega \cdot cm$) by using the *e*-beam evaporator (AUTO 306, Edwards). The wafer was then cut into samples with a size of $1 \times 1\ cm^2$ and the samples were loaded into the PECVD system. The dc PECVD reactor consisted of a suspended graphite cathode and a gas showerhead 5 cm above it. When the samples were heated to 800 °C by a tungsten heater embedded in the cathode, the cathode, biased negatively at a dc power of 80 W and a ratio of 240/60 sccm for NH_3/C_2H_2 at the pressure of 12 mbar, was used to grow CNT forests. NH_3 etching gas was used in the whole process to prevent the deposition of amorphous carbon phase. Vertically aligned CNTs are observed owing to the plasma-sheath controlled orientation in the PECVD process.[36−38]

The as-grown CNT forests were then processed by energetic Ar^+ ions by applying a negative pulsed bias at a voltage of −10 kV, a repetition rate of 500 Hz, and a pulse width of 20 μs.[17] The ion flux was focused by the bias and bombards the top but not the side walls of CNTs.[39,40] Ni nanoparticles melted because of heat generated in the process and protruded down along the CNT channel. Subsequently, the graphitic side walls of CNTs were partially smashed and spherical amorphous carbon (*a*-C) nanoparticles were formed on top of CNTs because of the nanotube amorphization induced by the energetic ions.[41] A typical process of fabrication of the *a*-C/CNT nanocomposites lasted approximately 10 min.

Scanning electron microscopy (SEM) images were taken using a JEOL JSM5910LV scanning electron microscope. Transmission electron microscopy (TEM) was carried out using a JEOL JEM2010 transmission electron microscope. The preparation of TEM samples was done by shaving the nanostructures on the surface layer off into ethanol and then dispensing the ethanol solution on the carbon-coated copper grids. The grids were then dried for TEM investigations. Contact angle measurements used the Dataphysics OCA 20 system. The sessile drop method was employed and the dynamic wetting processes can be recorded by a light source together with a camera.

Supporting Information Available: The schematic diagram of the plasma-aided system for fabricating *a*-C/CNT nanocomposites; the structure of *a*-C/CNT nanocomposites; the snapshots for the dynamic contact angle measurements on *a*-C/CNT nanocomposites; the schematic diagram demonstrating that the Cassie state is enabled with the "overhang" structure; the structure of a typical CNT forest and the corresponding contact angle measurements; and the time evolution of droplets evaporated with and without electrowetting. This material is available free of charge *via* the Internet at http://pubs.acs.org.

REFERENCES AND NOTES

1. Prins, M. W. J.; Welters, W. J. J.; Weekamp, J. W. Fluid Control in Multichannel Structures by Electrocapillary Pressure. *Science* **2001**, *291*, 277–280.
2. Yoshida, M.; Lahann, J. Smart Nanomaterials. *ACS Nano* **2008**, *2*, 1101–1107.
3. Song, W.; Veiga, D. D.; Custodio, C. A.; Mano, J. F. Bioinspired Degradable Substrates with Extreme Wettability Properties. *Adv. Mater.* **2009**, *21*, 1830–1834.
4. Zeira, A.; Chowdhury, D.; Maoz, R.; Sagiv, J. Contact Electrochemical Replication of Hydrophilic−Hydrophobic Monolayer Patterns. *ACS Nano* **2008**, *2*, 2554–2568.
5. Yuan, J.; Liu, X.; Akbulut, O.; Hu, J.; Suib, S. L.; Kong, J.; Stellacci, F. Superwetting Nanowire Membranes for Selective Absorption. *Nat. Biotechnol.* **2008**, *3*, 332–336.
6. Ostuni, E.; Chen, C. S.; Ingber, D. E.; Whitesides, G. M. Selective Deposition of Proteins and Cells in Arrays of Microwells. *Langmuir* **2001**, *17*, 2828–2834.
7. Yang, X.; Zhuang, J.; Li, X.; Chen, D.; Ouyang, G.; Mao, Z.; Han, Y.; He, Z.; Liang, C.; Wu, M.; Yu, J. C. Hierarchically Nanostructured Rutile Arrays: Acid Vapor Oxidation Growth and Tunable Morphologies. *ACS Nano* **2008**, *3*, 1212–1218.
8. Barthlott, W.; Neinhuis, C. Purity of the Sacred Lotus, or Escape from Contamination in Biological Surfaces. *Planta* **1997**, *202*, 1–8.
9. Roach, P.; Shirtcliffe, N. J.; Newton, M. I. Progess in Superhydrophobic Surface Development. *Soft Matter* **2008**, *4*, 224–240.
10. Wenzel, R. N. Resistance of Solid Surfaces to Wetting by Water. *Ind. Eng. Chem.* **1936**, *28*, 988–994.
11. Cassie, A. B. D.; Baxter, S. Wettability of Porous Surfaces. *Trans. Faraday Soc.* **1944**, *40*, 546–551.
12. Lafuma, A.; Quéré, D. Superhydrophobic States. *Nat. Mater.* **2003**, *2*, 457–460.
13. Londe, G.; Chunder, A.; Zhai, L.; Cho, H. J. An Analytical Model for the Wettability Switching Characteristic of a Nanostructured Thermoresponsive Surface. *Appl. Phys. Lett.* **2009**, *94*, 164104/1–164104/3.
14. Bormashenko, E.; Pogreb, R.; Whyman, G.; Bormashenko, Y.; Erlich, M. Vibration-Induced Cassie-Wenzel Wetting Transition on Rough Surfaces. *Appl. Phys. Lett.* **2007**, *90*, 201917/1–201917/2.
15. Wang, Z.; Lopez, C.; Hirsa, A.; Koratkar, N. Impact Dynamics and Rebound of Water Droplets on Superhydrophobic Carbon Nanotube Arrays. *Appl. Phys. Lett.* **2007**, *91*, 023105/1–023105/3.
16. Krupenkin, T. N.; Taylor, J. A.; Schneider, T. M.; Yang, S. From Rolling Ball to Complete Wetting: The Dynamic Tuning of Liquids on Nanostructured Surfaces. *Langmuir* **2004**, *20*, 3824–3827.

17. Han, Z. J.; Tay, B. K.; Shakerzadeh, M.; Ostrikov, K. Superhydrophobic Amorphous Carbon/Carbon Nanotube Nanocomposites. *Appl. Phys. Lett.* **2009**, *94*, 223106/1–223106/3.

18. Ostrikov, K. Reactive Plasmas as a Versatile Nanofabrication Tool. *Rev. Mod. Phys.* **2005**, *77*, 489–511.

19. Mugele, F.; Baret, J.-C. Electrowetting: From Basics to Applications. *J. Phys.: Condens. Matter* **2005**, *17*, R705–R774.

20. Chen, J. Y.; Kutana, A.; Collier, C. P.; Giapis, K. P. Electrowetting in Carbon Nanotubes. *Science* **2005**, *310*, 1480–1483.

21. Zhu, L.; Xu, J.; Xiu, Y.; Sun, Y.; Hess, D. W.; Wong, C.-P. Electrowetting of Aligned Carbon Nanotube Films. *J. Phys. Chem. B* **2006**, *110*, 15945–15950.

22. Ahuja, A.; Taylor, J. A.; Lifton, V.; Sidorenko, A. A.; Salamon, T. R.; Lobaton, E. J.; Kolodner, P.; Krupenkin, T. N. Nanonails: A Simple Geometrical Approach to Electrically Tunable Superlyophobic Surfaces. *Langmuir* **2008**, *24*, 9–14.

23. Lau, K. K. S.; Bico, J.; Teo, K. B. K.; Chhowalla, M.; Amaratunga, G. A. J.; Milne, W. I.; McKinley, G. H.; Gleason, K. K. Superhydrophobic Carbon Nanotube Forests. *Nano Lett.* **2003**, *3*, 1701–1705.

24. Wang, Z.; Ci, L.; Chen, L.; Nayak, S.; Ajayan, P. M.; Koratkar, N. Polarity-Dependent Electrochemically Controlled Transport of Water through Carbon Nanotube Membranes. *Nano Lett.* **2007**, *7*, 697–702.

25. Zhao, B.; Futaba, D. N.; Yasuda, S.; Akoshima, M.; Yamada, T.; Hata, K. Exploring Advantages of Diverse Carbon Nanotube Forests with Tailored Structures Synthesized by Supergrowth from Engineered Catalysts. *ACS Nano* **2009**, *3*, 108–114.

26. Pint, C. L.; Xu, Y.-Q.; Pasquali, M.; Hauge, R. H. Formation of Highly Dense Aligned Ribbons and Transparent Films of Single-Walled Carbon Nanotubes Directly from Carpets. *ACS Nano* **2008**, *2*, 1871–1878.

27. Wang, Z.; Koratkar, N.; Ci, L.; Ajayan, P. M. Combined Micro-/Nanoscale Surface Roughness for Enhanced Hydrophobic Stability in Carbon Nanotube Arrays. *Appl. Phys. Lett.* **2007**, *90*, 143117/1–143117/3.

28. Han, Z. J.; Morrow, R.; Tay, B. K.; McKenzie, D. Time-Dependent Electrical Double Layer with Blocking Electrode. *Appl. Phys. Lett.* **2009**, *94*, 043118/1–043118/3.

29. Kulinich, S. A.; Farzaneh, M. Effect of Contact Angle Hysteresis on Water Droplet Evaporation from Super-Hydrophobic Surfaces. *Appl. Surf. Sci.* **2009**, *255*, 4056–4060.

30. Wang, S.; Wang, D. Z.; Ji, L. J.; Gong, Q. M.; Zhu, Y. F.; Liang, J. Equilibrium and Kinetic Studies on the Removal of NaCl from Aqueous Solutions by Electrosorption on Carbon Nanotube Electrodes. *Sep. Purif. Technol.* **2007**, *58*, 12–16.

31. Mani, R. C.; Li, X.; Sunkara, M. K.; Rajan, K. Carbon Nanopipettes. *Nano Lett.* **2003**, *3*, 671–673.

32. Cvelbar, U.; Chen, Z.; Sunkara, M. K.; Mozetic, M. Spontaneous Growth of Superstructure a-Fe_2O_3 Nanowire and Nanobelt Arrays in Reactive Oxygen Plasma. *Small* **2008**, *4*, 1610–1614.

33. Fletcher, B. L.; Retterer, S. T.; McKnight, T. E.; Melechko, A. V.; Fowlkes, J. D.; Simpson, M. L.; Doktycz, M. J. Actuatable Membranes Based on Polypyrrole-Coated Vertically Aligned Carbon Nanofibers. *ACS Nano* **2008**, *2*, 247–254.

34. Levchenko, I.; Rider, A. E.; Ostrikov, K. Control of Core-Shell Structure and Elemental Composition of Binary Quantum Dots. *Appl. Phys. Lett.* **2007**, *90*, 193110/1–193110/3.

35. Cvelbar, U.; Ostrikov, K.; Drenik, A.; Mozetic, M. Nanowire Sensor Response to Reactive Gas Environment. *Appl. Phys. Lett.* **2008**, *92*, 133505.

36. Levchenko, I.; Ostrikov, K.; Long, J. D.; Xu, S. Plasma-Assisted Self-Sharpening of Platelet-Structured Single-Crystalline Carbon Nanocones. *Appl. Phys. Lett.* **2007**, *91*, 113115.

37. Keidar, M.; Levchenko, I.; Arbel, T.; Alexander, M.; Waas, A. M.; Ostrikov, K. Increasing the Length of Single-Wall Carbon Nanotubes in a Magnetically Enhanced Arc Discharge. *Appl. Phys. Lett.* **2008**, *92*, 043129/1–043129/3.

38. Mariotti, D.; Švrček, V.; Kim, D.-G. Self-Organized Nanostructures on Atmospheric Microplasma Exposed Surfaces. *Appl. Phys. Lett.* **2007**, *91*, 183111/1–183111/3.

39. Levchenko, I.; Ostrikov, K. Nanostructures of Various Dimensionalities from Plasma and Neutral Fluxes. *J. Phys. D: Appl. Phys.* **2007**, *40*, 2308–2319.

40. Tam, E.; Levchenko, I.; Ostrikov, K. Deterministic Shape Control in Plasma-Aided Nanotip Assembly. *J. Appl. Phys.* **2006**, *100*, 036104/1–036104/3.

41. Wei, B. Q.; D'Arcy-Gall, J.; Ajayan, P. M.; Ramanath, G. Tailoring Structure and Electrical Properties of Carbon Nanotubes Using Kilo-Electron-Volt Ions. *Appl. Phys. Lett.* **2003**, *83*, 3581–3583.